Evaluating freckle tendency for electro-slag remelting 30CrMnSiNi2A ingots by experiments and simulation

Y. Zhang, W. Q. Chen, L. Chen , Q. Z. Yan, C. W. Li

The mechanisms and tendency of freckle formation in industrial scale ESR ingots were studied by thermodynamic calculation, thermo-physical property calculation, metallographic observation, and composition analysis. The macrostructure and compositions of the freckle regions in a low alloy ultrahigh strength ESR steel ingot were investigated to clarify the freckle formation mechanism. Combining the results with composition analysis and thermodynamic calculation, it can be concluded that the compositions of freckles correspond to that of liquid with a liquid fraction of 0.24 to 0.41, and the freckles were caused by the upward solute-rich liquid flow which initiate at the lower part of mushy zone. The relative Rayleigh number (Ra), a freckle criterion considering the effect of a tilted solidification front, was adopted to evaluate the freckle formation tendency in the industrial scale ESR ingots. The calculated results of Ra numbers of different locations are in good agreement with the actual distribution of the freckles in the ingot.

INTRODUCTION

Thermosolutal convection due to thermal and compositional variation can cause the formation of freckles (channel-like macrosegregation defects). Freckles are commonly observed in cast alloy or steel ingots, such systems generally contain two or more alloying elements with different densities and phases [29]. Freckles appear as long liner trails of misoriented dendrites with a composition shift consistent with alloy segregation. Generally, freckles in full size ingot have a size from several millimeters to one centimeter in diameter, which at least 2 or 3 orders of magnitude larger than that of microsegregation. Freckles are highly undesirable in critical applications because of their deleterious effect on mechanical performance, such as tensile, fracture toughness, and fatigue crack growth are significantly degraded when the longitudinal direction of the freckle channels is perpendicular to the loading axis. The hardness of the freckle region is much higher than that of matrix since some alloying elements enriched in freckle regions, then micro-cracks may formed from the interfaces between the freckles and matrix. The freckles cannot be removed by any heat treatment once it has formed in a fully solidified casting [1-4].

Yang Zhang, Weiqing Chen

State Key Laboratory of Advanced Metallurgy, University of Science and Technology Beijing, Beijing 100083, China

Lie Chen, Qingzhong Yan, Chengwei Li

Xining Special Steel Co., LTD., Xining 810005, China

It is generally agreed that the formation of the freckles is due to a complex interaction of solute segregation, thermal variation and dendrite morphology, all of which contribute to the onset of thermosolutal convection in the mushy zone [1]. The probability of the frcekle formation during the electro-slag remelting (ESR) process is mainly dependent on the following factors: the alloy composition, the solidification parameters (melting rate of electrodes, radial heat extraction, and cooling intensity, et), the defects of electrode (for example, the perturbations of the melting rate can be resulted from using of the electrodes with internal cracks, which promote the thermosolutal convection in the mushy zone), and the casting size [15-18].

Many efforts [1-20] have been made on the mechanism and criterion of freckle formation since the macrosegregation theory was proposed by Flemings and his co-workers [5-6]. However, few investigations have been focused on the freckle defects of the electro-slag remelting (ESR) ingots [4,15-20]. Previous researches ignored the effects of the variation of liquid viscosity on the interdendritic liquid flow, the back diffusion of interstitial elements in solid on the liquid composition and the solidification temperature range. For example, the solidification temperature range calculated by Scheil-Gulliver equation (where no back-diffusion is considered) is generally 100-300°C larger than that of the actual solidification for steels. Thus the above two factors will be considered in this investigation.

This study aimed at enhancing the fundamental understanding of the freckle formation mechanism and tendency evaluation during the ESR solidification process

by experimental investigations and simulated calculation. The thermodynamic calculation software (Thermo-Calc) and Java-based materials properties software (JMatPro) were used to predict the variation of liquid composition, density, and viscosity during the solidification. Finally, a Rayleigh number criterion that represents the ratio of the driving force for the interdendritic liquid flow and the resistance for the flow, it is appropriate to describe the instability convective flow phenomenon in the mushy zone according to the theory of thermosolutal convection [20]. This criterion includes the effect of liquid composition and viscosity variation, the slope of the solidification front, permeability of the mushy zone, and the cooling conditions, was adopted to evaluate the freckle tendency of industrial scale ESR ingots.

EXPERIMENTAL PROCEDURES

A 720-mm-diameter ingot of 30CrMnSiNi2A was produced on an industrial-scale ESR furnace, the chemical composition of the steel is shown in table 1. The electrodes with a 400-mm diameter used for the ESR process was produced by vacuum-induction melting (VIM). A 30-mm-thick slice for macro etching was sectioned along the longitudinal centerline of the ESR ingot. The slice was etched using 50 pct HCl-50 pct H_2O to reveal freckles. Then 25 cube samples with a dimension of 30mm × 30mm × 30mm for dendrite etching was prepared along the radial direction and the axial direction of the slice, the sampling locations of the radial direction are edge, 2/3-radius, 1/2-radius, 1/3-radius, and centre, and the sampling locations of the axial direction are top, 3/4-height, middle, 1/4-height, and bottom, the method is illustrated in Fig. 1. The 25 samples were etched by 5 pct trinitrophenol to reveal the dendritic structure, and the secondary dendrite arm spacing (SDAS) was measured using the image analysis software ImageTool (Version 3.0, Department of Dental Diagnostic Science at The University of Texas Health Science Center, San Antonio, Texas). Meanwhile, two samples for the freckles analysis were cut from the top and the bottom of a freckle channel (as Fig. 2 shows). An EVO 18 scanning electron microscope (SEM, Carl Zeiss Microscopy GmbH, Jena, Germany) equipped with energy dispersive X-ray spectrometer (EDS) was used to acquire analytical composition data in the second electron image (SEI) mode. And the same samples (as-polished) were also used for measuring the microhardness by a LEICA VMHT 30M type Vickers microhardness tester with the applied load 50 g and the loading time 15 s.

THERMODYNAMIC AND THERMO-PHYSICAL APPROACHES

Thermodynamic calculation
Based on the Scheil-Gulliver model [25,26], the traditional-Scheil module has been implemented inside Thermo-Calc
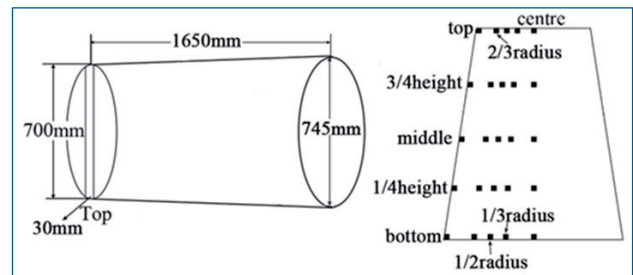

Fig. 1 - Schematic diagram of the sampling positions

C	Si	Mn	P	S	Cr	Ni	Cu	Ti	Al
0.30	1.05	1.09	0.015	0.003	1.03	1.62	0.06	0.018	0.063

Table 1 - Chemical compositions of 30CrMnSiNi2A steel, wt%

software. The module assumes that solute elements diffuse rapidly within the liquid phase and that diffusion in the solid phases is negligible. Along each step in the cooling process, local equilibrium is established at the solidification interface where the compositions of liquid and solid are given by the system's phase diagram [17].
On the basis of the traditional-Scheil module, one or more fast diffusing elements (usually interstitial elements such as C, N, O, S, and B) can be defined in the modified-Scheil module, thus their back diffusion in solid phases can be taken into account during a simulation. The back diffusion of interstitial elements in solid phases is complete, but that of substitutional elements is negligible. Interstitial elements are allowed to diffuse freely among the liquid and all portions of the solid phases formed, and substitutional elements are completed limited in the remaining liquid and each portion of the solid phases formed [18]. And for steels with primary ferrite, the transition from δ-ferrite to austenite can be considered in this module, such a transformation will change the chemical potentials of interstitial elements and thus influence their back diffusion in solid phases.
Then, the modified-Scheil module of Thermo-Calc software was used to predict the composition and the density of the liquid during the solidification, and the alloy composition was assumed to be Fe-0.3C-1.05Si-1.09Mn-1.03Cr-1.62Ni-0.015P here. Meanwhile, C and P were defined as the fast diffusing elements, and the transition from δ-ferrite to austenite during peritectic reaction was also considered.

Thermo-physical property calculation
Java-based materials properties software (JMatPro) provides extensive information on how the properties of an alloy or each individual phase may change within its specification range, such as the liquid phase in the mushy zone, which is usually beyond the capability of measurement [19]. For each individual phase in multi-component systems, properties can be calculated by

$$P = \sum_i x_i P_i^0 + \sum_i \sum_{j>i} x_i x_j \sum_v \Omega_{ij}^v (x_i - x_j)^v \qquad (1)$$
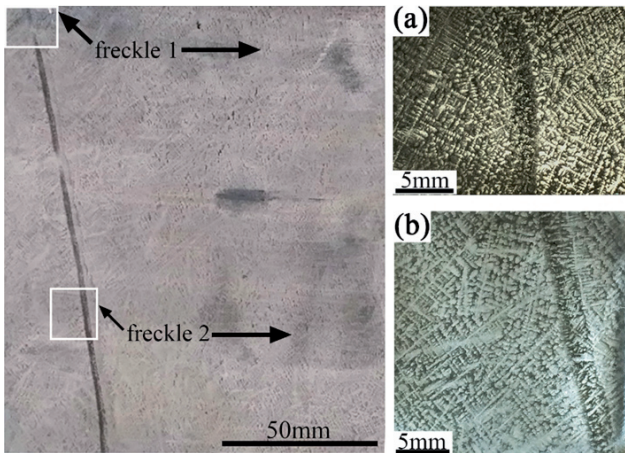
Fig. 2 -Macrostructure of the freckle in the 30CrMnSiNi2A steel ingot: (a) freckle 1; (b) freckle 2

Fig. 3 - The relation of fluid flow and dendrite growth at a tilted solidification front

Where, P is the property of the phase, P_1^0 is the property of the phase in the pure element, $Ù_{ij}^v$ is a binary interaction parameter dependent on the value of v, x_i and are the mole fractions of elements i and j in the phase. Both P_1^0 and $Ù_{ij}^v$ are temperature dependent and it is possible to include ternary or higher order effects where appropriate [20].

The General Steel solidification properties module of JMatPro software was used to calculate the variation of liquid viscosity during the solidification in this research. The starting temperature of the continuous cooling process was set at 1600 °C and a cooling rate of 0.1°Cs^{-1} was chosen. In addition, C and P were defined as interstitial elements, and the alloy composition used in this calculation is shown in Table 1. First, the amount and composition of liquid in this steel is calculated based on thermodynamics and phase transformation kinetics, and the back diffusion of interstitial elements is also considered in this calculation, then the property of liquid can be calculated by Eq. (1). For the case of steels, interstitial elements diffuse rapidly in the solid state and it is possible to consider that complete back diffusion of interstitial elements will occur. Such a model has been implemented in JMatPro by considering that interstitial elements will diffuse sufficiently rapidly so that their composition in the growing austenite or ferrite phases will be equal to that of the solid at the growing solid/liquid interface [28].

RESULTS AND DISCUSSION

Macrostructure of freckle
During solidification, solute elements are rejected from the dendrites and their concentration gradually increases in the interdendritic region. Si, Mn, Cr is lighter than Fe, and therefore natural convection is initiated and the interdendritic liquid flows upwards. The interdendritic segregated liquid is solute-rich, both flowing upwards due to buoyancy forces and altering the local free energy driving force for solidification. Since the segregated liquid
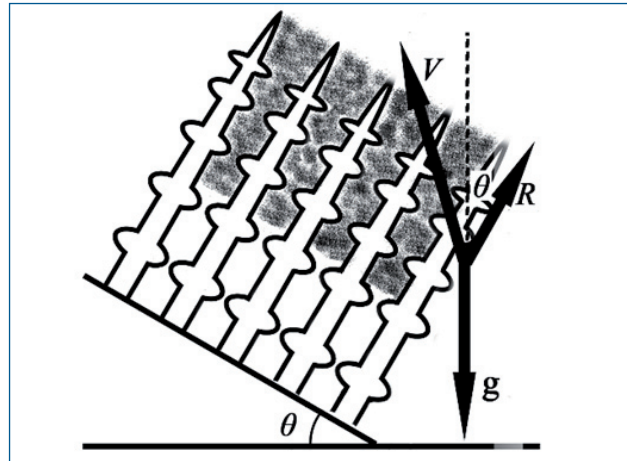
has higher solute concentration, it can reduce the local undercooling and, thereby retard the growth of dendrites. As a consequence, the dendrite arms in the segregation channel can remelt, potentially sustaining the formation of the segregation channels. There is also an additional force on the arms in the segregation channel, upward flow. This flow will produce surface shear on the arms, which will concentrate as a bending moment at the neck of dendrite arms. By this way, both primary and secondary arms in the channel were etched/melted.

The freckles were only found in the 1/2-radius region from the upper part (from about 2/5-height to the top) of the ingot, but not in the centre region. Two samples marked by the white rectangles (Fig. 2) were cut from the top and the bottom of a freckle channel in order to reveal the dendritic structure and measure the composition of the freckle, the two regions were referred to as "freckle 1" and "freckle 2". The right part of Fig. 2 gives the dendritic structure of freckle 1 and freckle 2. It shows the growth direction of the primary dendrites is basically same with the thermal gradient direction, is from left-bottom to top-right. The freckles are basically running from bottom to top but slightly leaning from right to left.

When thermosolutal convection starts, partitioning of the lighter solute elements cause the interdendritic fluid to advect out of the interdendritic region. Owing to the conservation of continuity, the channel draws segregated liquid from the neighbouring interdendritic regions. Then the solute-rich liquid flows upward through the mushy zone into the liquid layer, the upward flow of solute-rich liquid is accompanied by a downward flow of solute-lean liquid to ensure the conservation of volume [29]. Thus the concentration of solute elements in the channel gradually decreases along the flow direction of solute-rich liquid, consequently, the velocity inside the ascending segregated liquid and the ability of solute-rich liquid to etch/remelt dendrite arms also decreases. It can be obviously seen from Fig. 2b that there is a misoriented dendritic structure in the freckle 2, which is very different from the surrounding

Element	Si	Mn	Cr	Ni	HV (Mpa)
Freckle	1.46	1.59	1.44	1.89	365.5
Matrix	1.10	1.20	1.15	1.61	275
SD	0.05	0.11	0.12	–0.01	...
Average error	±0.2	±0.2	±0.1	±0.2	...

Tab. 2 - Compositions of freckle 2 and the surrounding area, wt-%
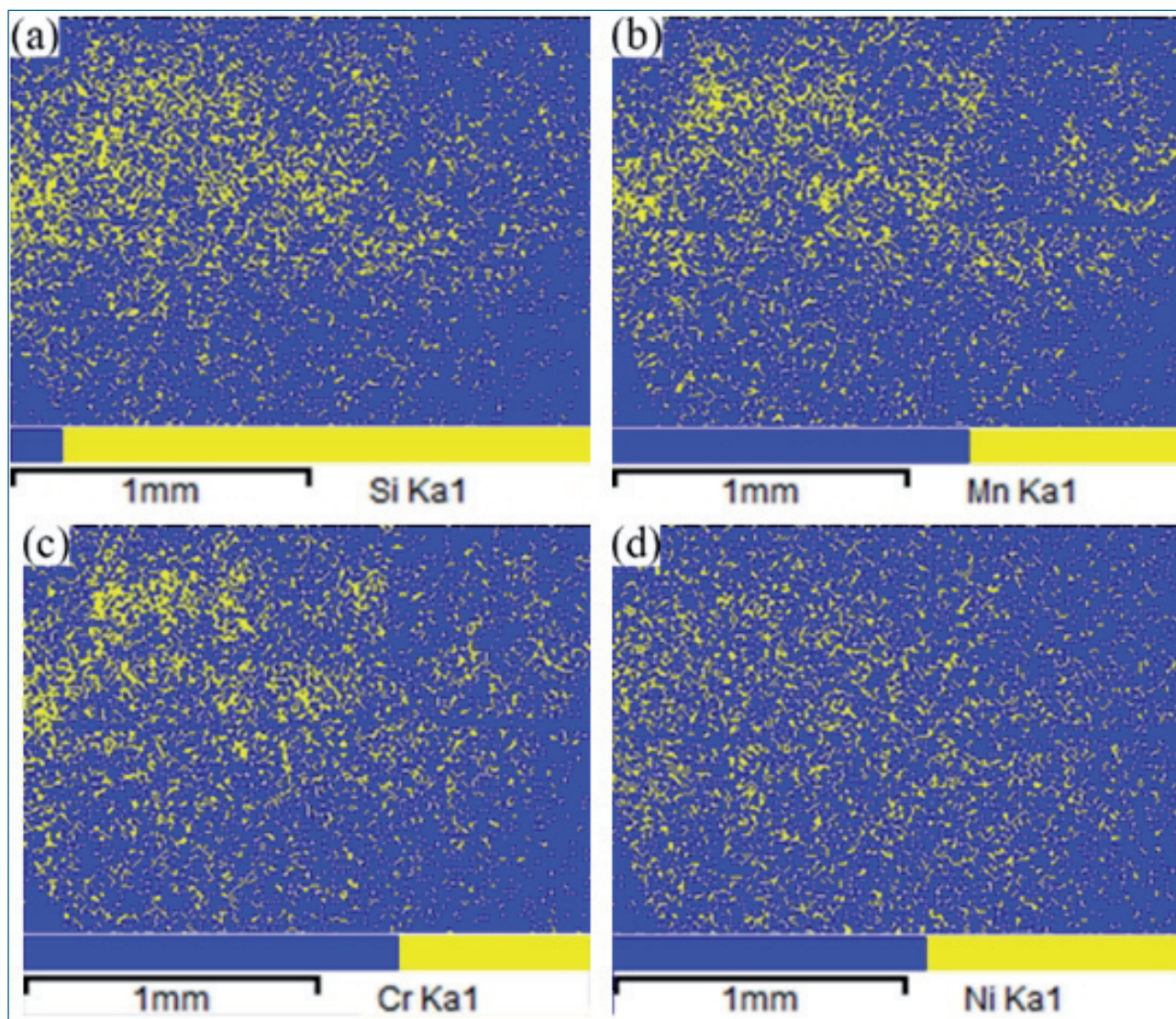

Fig. 4 - The elements distribution map of the freckle region (upper-left part) and the matrix: (a) Si, (b) Mn, (c) Cr, and (d) Ni

matrix. However, the dendrite morphology in the freckle 1 is basically same as that in the surrounding matrix, only part of dendrites in the freckle 1 (Fig. 2a) were etched/melted. The obvious difference of the dendrite morphology between the freckle 1 and freckle 2 confirmed that the upward solute-rich liquid flow is the reason of freckles formation in the 30CrMnSiNi2A ESR ingots, the liquid flow in the bottom of a freckle channel is stronger than that in the top, thus the original dendritic structure in the freckle 2 was etched/melted completely, The flow during remelting may be sufficient to break off the dendrite arms in the segregation channel. These are heavier and hence may fall, as the fragments fall the temperature around them decreases, and some may reach equilibrium before completely remelting, which acting as pre-existing nuclei to form the classic misoriented dendritic structure observed experimentally.

Fig. 3 shows the relation between fluid flow and dendrite growth in the mushy zone. The solidification front which has an angle θ to the horizontal plane is represented

	edge	2/3-radius	1/2-radius	1/3-radius	Centre
top	46	38	40	26	20
3/4-height	64	38	35	20	10
middle	50	35	35	30	25
1/4-height	65	45	40	28	16
bottom	65	60	50	23	18

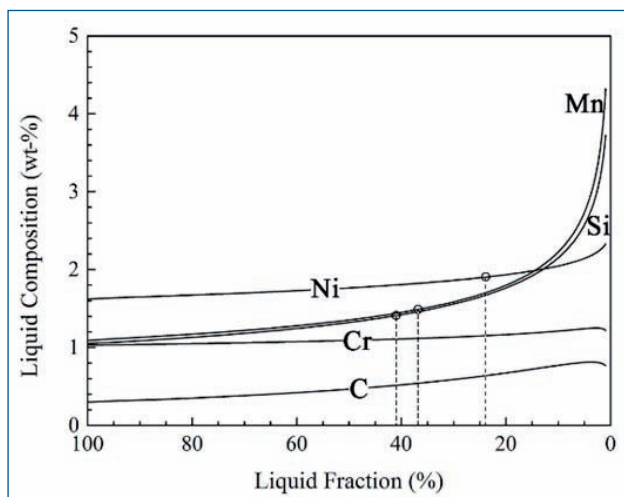*Tab. 3 - Solidification front angle at different locations (deg)*

Fig. 5 - Liquid composition as function of Liquid Fraction during the solidification

by the isotherm (isodensity), which is perpendicular to the dendrite growth direction of the primary dendrites. R is the growth velocity, g is the gravity. The flow of the interdendritic solute-rich liquid is represented by V. For this steel, the flow of the solute liquid was observed to closely follow the vertical direction at a small angle of deviation.

The formation of the freckles is a result of the thermosolutal convection in the mushy zone. The main factors affecting the thermosolutal convection are the thermal gradient, the permeability in mushy zone, and the liquid density difference. The dendrites growth direction is determined by the thermal gradient. On the other hand, the flow of the interdendritic fluid was limited by the dendritic structure, considering the freckle formation as a case of solute-rich liquid flow in a porous media, then the permeability is a key parameter that affects the flow velocity within the mushy zone. In addition, solute elements are ejected from solid into liquid during the solidification, the liquid composition in the vicinity of the dendrite bottom is different from that of dendrite tip. Such liquid density difference plays a key role in driving the interdendritic thermosolutal convection and the freckle formation.

Inside the mushy zone, the buoyancy forces may become sufficiently strong to overcome the resistance offered by the dendritic structure as an increase in the liquid density difference and a decrease in the liquid viscosity, and upward flow of solute-rich liquid will occur. Because the permeability for liquid flow perpendicular to the primary dendrites is 2.5 to 4 times greater than that parallel to the primary dendrites [25,26], thus the interdendritic solute-rich liquid tends to flow along the path which offers lower resistance. It is therefore suggested that, under similar solidification conditions, a tilted solidification front should favor of upward flow of the interdendritic liquid, while a horizontal solidification front is freckle-free. As Fig. 3 shows, the interdendritic solute-rich liquid preferentially flows along a low resistance path that has an angle to the vertical direction, which is the result of the competition between the driving force of flow offered by the liquid density difference and the resistance from the dendritic structure in the mushy zone. The interdendritic solute-rich liquid would retain its composition and remelt/erode the already formed dendritic structure when it flows upward to higher temperature positions, because the solute diffusivity in the liquid is much lower than the thermal diffusivity.

MICROSCOPIC CHARACTERISTICS OF FRECKLE

Freckle composition
A polished but unetched freckle sample was analyzed by SEM/EDS. The compositions of the freckle region and its surrounding matrix, with standard deviation (Standard deviation is the difference between the compositions of the matrix of freckle region and chemical compositions of this steel (as Table 1 shows)), is shown in Table 2. The results are the average compositions from the measured results at least five different locations. Considering the average compositions of the matrix should equal to the chemical compositions of this steel, the measured compositions of the freckle region can be modified by standard deviation (SD). Fig. 4 shows the elements distribution map of the freckle region and its surrounding matrix measured by EDS. It can be seen from Table 2 and Fig. 4 that the freckle region is enriched with Si, Mn, and Cr compared with the surrounding matrix. Among these elements, the segregation of Mn is the largest, and that of Ni is the least.

The Vickers microhardness value of the freckle region and the surrounding matrix are shown in the right part of Table 2. It can be seen that the microhardness in the freckle region is 33% higher than the surrounding matrix, micro-cracks may form from the interfaces between the freckles and the matrix when steel subjected to mechanical and thermal loadings.

Secondary dendrite arm spacing (SDAS) and solidification front angle

Fig. 8a shows the measured secondary arm spacing 2 (µm) at different locations of the ingot. It can be seen that the maximum SDAS occurs at the location of 1/2-radius, and the SDAS increases as the height of the ingot increases. The joint cooling intensity of the bottom water tank and mold, its maximum value occurs in the bottom, thus the dendritic structure in the bottom is the finest, and that in the top is the coarsest. Table 3 shows the solidification front angle at different locations of the ingot, the results were obtained by measuring the angle between growth direction of primary dendrites and vertical direction (Fig. 3). The maximum error in the determination of solidification front angles is ±1 deg. It can be concluded that the tendency of freckle formation increases as the increase of SDAS and that of solidification front angle, thus solidification conditions in the 1/2-radius region from the upper part of the ESR ingot is favor of the freckle formation.

THERMODYNAMIC AND THERMO-PHYSICAL APPROACHES TO CALCULATE THE RA

Liquid composition during the solidification

Fig. 5 shows the relation between the liquid composition and liquid fraction, which was calculated by the modified–Scheil module of Thermo-Calc software. It can be seen that the liquid composition has an obvious change during the solidification. The concentrations of Mn and Si increases dramatically as the liquid fraction decreases, but the concentration of Ni have a minor increase. The density of Mn, Si, and Cr is less than Fe, which being enriched in interdendritic liquid result in the decrease in the liquid density. Comparing the concentration profiles of interdendritic liquid (Fig. 5) with the modified compositions of the freckle region (Table 2), it can be observed that the segregation level of Cr was underestimated in the thermodynamic calculation, but the calculated results of Mn, Si, and Ni are reasonable. Therefore, the correspondent liquid fraction of freckle compositions was determined from the segregation profiles of Mn, Si, and Ni, this method is illustrated in Fig. 5. The compositions of freckles in the 30CrMnSiNi2A ingot correspond to a range of liquid fraction 0.24-0.41.

Density and viscosity of the liquid during the solidification

The variation of the liquid density during the solidification can be estimated with a relative high accuracy in modified–Scheil module by considering the effects of the volume shrinkage, the composition change, the phase transition, and the back diffusion of interstitial elements, etc. The difference between the density at the liquidus temperature (liquid fraction fL = 100) and the density at a temperature T (TS≤T≤TL, Where TL and TS are the liquidus and solidus temperature, respectively), represented by Δρ. Fig. 6a shows the variation of liquid density during the solidification, it can be seen that the liquid density difference increases dramatically as the liquid fraction decreases.

The effects of composition and temperature on viscosities of liquid alloy can be estimated by the following equations [24]:

$$\eta = A\exp\left(B/RT\right)$$

$$A = \frac{1.7 \times 10^{-7} \rho_L^{2/3} T_m^{1/2} M^{-1/6}}{\exp(B/RT_m)} \tag{2}$$

$$B = 2.65 T_m^{1.27}$$

Where ρ_L is the liquid density of alloy (kg·m^{-3}), is the absolute liquidus temperature *(K)*, *M* is molar mass (kg·mol^{-1}), and *R* is gas constant (8.3144 J·mol^{-1}·K^{-1}).

Liquid viscosity affects the flow velocity of interdendritic liquid, it is very important to obtain reliable data of the liquid viscosity for the investigation of the liquid flow behavior in the mushy zone. While it is impossible to measure the liquid viscosity directly, Fig. 6b shows the variation of the liquid viscosity calculated by the General Steel solidification properties module of JMatPro software, it can be seen that the liquid viscosity decreases as the liquid fraction decreases, which means that the flow velocity of the interdendritic liquid increases.

Calculated results of relative Rayleigh number

The permeability is a key parameter that affects the flow velocity within the mushy zone, and is the parameter that is associated with the region of interdendritic channels [26]. The permeability in the mushy zone represents the resistance to the interdendritic liquid flow, which is offered by dendritic structure and mainly affected by the liquid fraction and the dendritic morphology. Poirier [25] has developed the following expressions to estimate the permeability for a flow parallel and normal to the primary dendrites, K_P and K_N, respectively.

$$K_P = 3.75 \times 10^{-4} f_L^2 \lambda_1^2 \qquad for\ 0.17 \le f_L \le 0.61 \tag{3}$$

$$K_N = 3.62 \times 10^3 f_L^{3.34} \lambda_1^{0.699} \lambda_2^{2.73} \qquad for\ 0.19 \le f_L \le 0.66 \tag{4}$$

Where, K_P and K_N are the permeability components in the parallel and perpendicular directions to the primary dendrites, respectively, f_L is the liquid fraction, λ1 is the primary arm spacing, λ2 is the secondary arm spacing.

M. EL-Bealy and B.G. Thomas [27] proposed the following equation for estimating the primary and secondary dendrite arm spacing of low alloy steel, the cooling rate C_R (°Cs^{-1}) can be calculated by the Eq. (5).

$$\lambda_2 = 148(C_R)^{-0.38} \qquad for\ 0 \le C_0 \le 0.53\ (wt\ pct\ C) \tag{5}$$

$$\lambda_1 = 278.748 C_R^m C_0^n \qquad for\ 0.15 \le C_0 \le 1.0\ (wt\ pct\ C) \tag{6}$$

Where C0 (wt pct) is the average carbon content of this alloy, m = -0.206277638, n = -0.1663998.

It is difficult to measure the primary arm spacing for the ESR ingots directly, but CR can be calculated by Eq. (5)

Fig. 6 - The variation of the liquid density and liquid viscosity during the solidification: (a) Liquid density; (b) Liquid viscosity
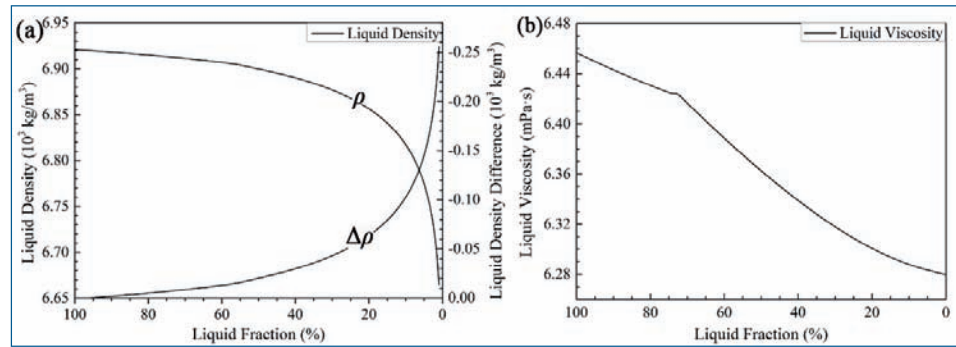
according to the measured values of the SDAS, then the primary arm spacing can be calculated by Eq. (6).

It is well known that the freckle is caused by the flow of the solute-rich liquid in the mushy zone during the solidification. The flow of the solute-rich liquid in ESR ingots is mainly affected by the variation of the liquid composition and the liquid viscosity, the mushy zone permeability, the solodification front angle, and the cooling conditions. A criterion that includes the above factors developed by Jairo Valdés et [4]. was found to predict the freckle formation satisfactorily. Rayleigh number (Ra), as given in Eq. (7).

$$Ra = (\frac{\Delta \rho\, g \cos \theta}{\nu f_L})(\frac{K_P^2 \cos^2 \theta + K_N^2 \sin^2 \theta}{R})^{\frac{1}{2}} \qquad (7)$$

Where ν is the dynamic or absolute viscosity of the interdendritic liquid; R is the dendrite growth rate. In this study, the dendrite growth rate was replaced by the cooling rate due to no reliable data being available, thus a simplified equation (Eq. (8)) was used to calculate the Ra, in order to distinguish the Rayleigh number (Ra) in the these two equations, the Rayleigh number (Ra) in Eq. (8) was named relative Ra.

$$Ra = (\frac{\Delta \rho\, g \cos \theta}{\nu f_L})(\frac{K_P^2 \cos^2 \theta + K_N^2 \sin^2 \theta}{C_R})^{\frac{1}{2}} \qquad (8)$$

Fig. 7 gives the calculated relative Ra number of 30CrMnSiNi2A, the negative value means that the liquid density difference is negative. The absolute value of Ra is proportional to the tendency for freckle formation. Along the axial direction of the ingot, the bottom had the maximum cooling rate, and correspondingly, its relative Rayleigh number was the lowest. The relative Rayleigh number in the middle region of the ingot are lower than that in the top region due to the fact that the cooling intensity is gradually to decreases as the height increases, it can be confirmed by the fact that the maximum SDAS occurs in the top region, and the freckles were only found in the upper part (from about 2/5-height to the top) of the ingot. Along the radial direction of the ingot, the maximum relative Rayleigh number occurs in the 1/2-radius region. Similarly, the freckles was only found in the 1/2-radius region but not the centre of ingot. Compare with other regions, the upward flow of the interdendritic fluid in the centre region is very difficult because the solidification

front is basically horizontal.

The liquid density difference increases and the liquid viscosity decreases, respectively, as the liquid fraction decreases, but the permeability in the mushy zone decreases, which means that the driving force, flow velocity, and the resistance to the interdendritic liquid flow increase at the same time. The interdendritic liquid could no longer flow when the liquid fraction decrease to within a specific range, because it is fully surrounded by solid. The tendency to form freckle in a steel is related to maximum Ra number through solidification. For this steel, the maximum relative Rayleigh number occur at 0.36-0.39 liquid fraction due to the competition between the driving force and the resistance of liquid flow, this result is basically consistent with the liquid fraction range determined by the compositions of the freckle.

From the above analysis, it can be found that a fine dendritic structure and a small solidification front angle are the key factors for preventing the freckles formation. The finer the dendritic structure, the lower the permeability in mushy zone and the higher the dendrite growth rate. Correspondingly, the segregation level of the interdendritic liquid is low, thus the liquid density difference is low. On the other hand, a small solidification front angle means the resistance to the upward liquid flow is lower than that of a large solidification front angle, this is due to the permeability anisotropy in the mushy zone. For the ESR process, a fine dendritic structure and a small solidification front angle can be obtained by reducing the melting rate, increasing the cooling intensity, improving heat transfer of the radial direction, increasing the fill ratio, and reducing the height of the ingot, etc.

It can be observed from Fig. 7 that for a 30CrMnSiNi2A ESR ingot, it is feasible to identify a threshold value of the Rayleigh number that gives a clear boundary between the freckle and non-freckle conditions. The threshold value of the Rayleigh number was defined as Ra*, below which there is no freckles formation. For 30CrMnSiNi2A, the estimated threshold Rayleigh number Ra* was about –0.12 according to the present calculated results.

The tendency to form freckle in an ingot is related to maximum Ra number through solidification. Fig. 8 shows the comparison between the secondary dendrite arm spacing and maximum Ra numbers at different locations of the ingot, it can be seen that the variation tendency of maximum Ra is basically as same as that of SDAS (secondary dendrite arm spacing), since the SDAS of as-
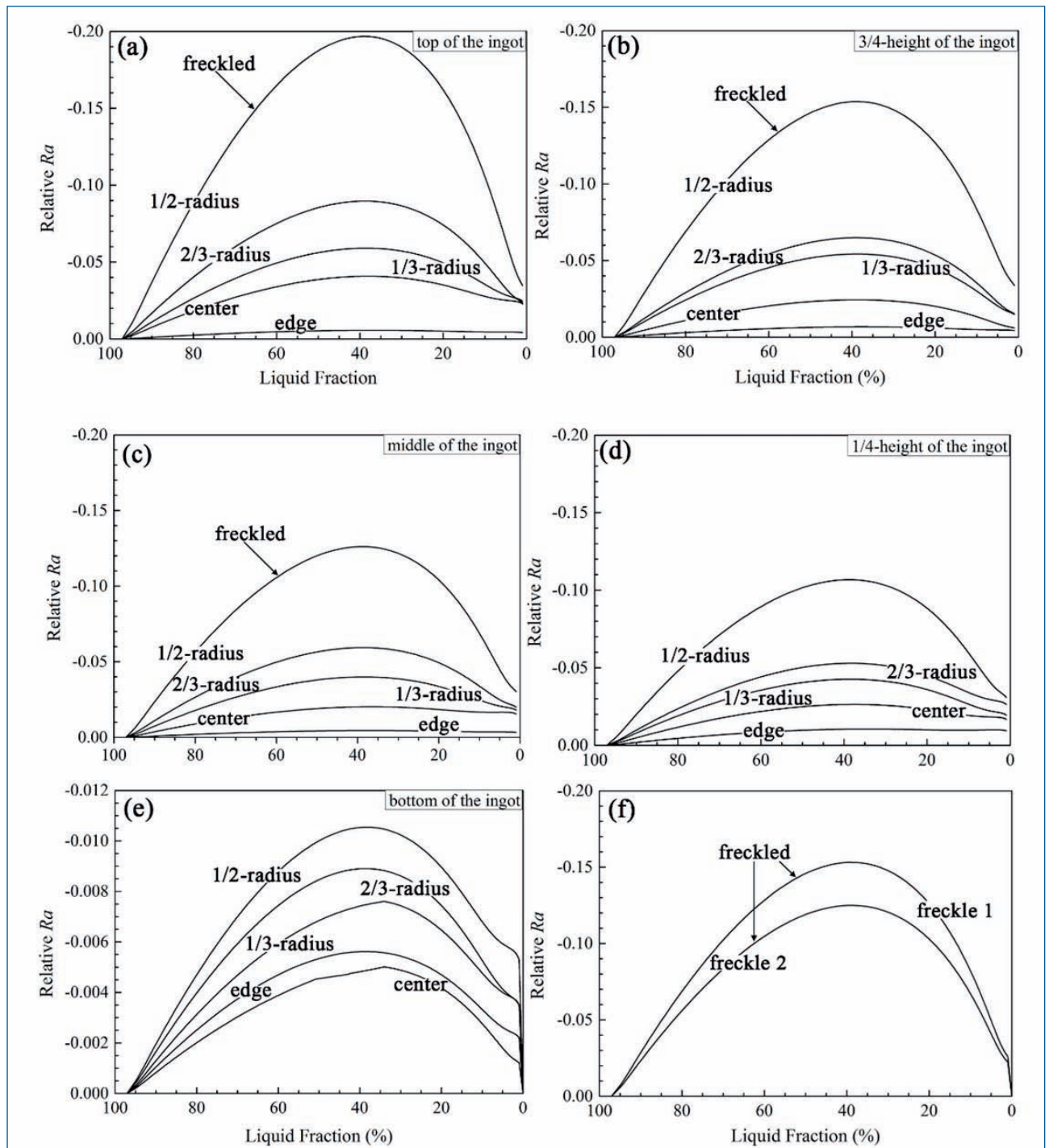
Fig. 7 - Relative Ra numbers at different location of 30CrMnSiNi2A steel ingot: (a) top of the Ingot, (b) 3/4-height of the ingot, (c) middle of the ingot, (d) 1/4-height of the ingot, (e) bottom of the Ingot, and (f) freckle 1 and freckle

cast ingots is inversely proportional to the cooling rate, and the cooling rate in ESR ingots is mainly determined by the melting rate of electrodes. High melting rate causes a deep pool profile, extends the mushy zone, and induces a stronger electromagnetic force field. Therefore, melting rate is the critical operating parameter for controlling the formation of freckles.

CONCLUSIONS

Thermodynamic and thermo-physical property calculation were coupled with the metallographic observation and composition analysis of an as-cast ESR steel ingot to investigate the mechanisms of freckle formation and evaluate the freckle tendency in industrial scale ESR ingots, using this method the following conclusions were drawn.

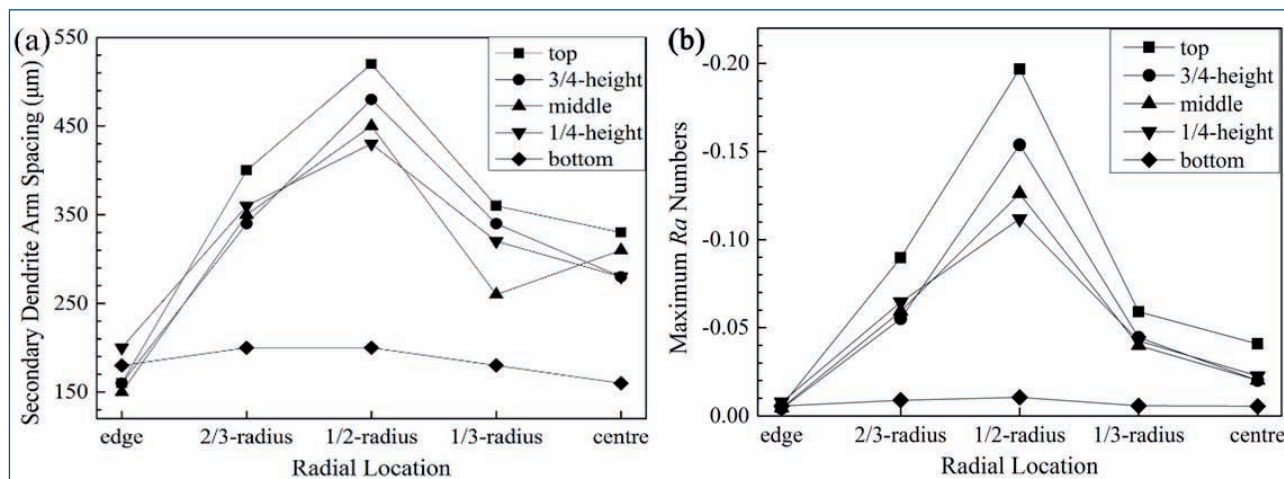1) Freckles enriched with Mn, Si, and Cr compared with

Fig. 8 - SDAS and Maximum Ra Numbers at different locations of the ingot: (a) SDAS; (b) Maximum Ra Numbers

the matrix, these were only found in the 1/2-radius region from the upper part of the 30CrMnSiNi2A ingot. And the microhardness in defect freckle region is much higher than that in surrounding matrix.

2) Freckles are mainly caused by the upward solute-rich liquid flow in mushy zone which would etch/remelt the dendrite arms inside the segregation channels, and this mechanism is confirmed by the dendritic micrographs of freckles in the ingot. Meanwhile, the direction of interdendritic liquid flow is strongly influenced by the permeability anisotropy in mushy zone.

3) The freckles in 30CrMnSiNi2A ingot has a composition corresponding to the interdendritic liquid with a liquid fraction of 0.24 to 0.41. This result is compared to the liquid fraction range where the calculated maximum Ra appears, and the calculated results have shown good agreement with experiment, thus the freckles in ESR ingots initiate at the lower part of mushy zone.

4) The effect of the liquid composition variation on the density and viscosity of liquid can be explicitly analysed by combining the thermodynamic calculation with thermo-physical property calculation.

REFERENCES

[1]   L. Yuan, P. D. Lee, "A new mechanism for freckle initiation based on microstructural level simulation", Acta Materialia, 60 (12) pp. 4917-4926, 2012.

[2]   P. Auburtin, T. Wang, S. L. Cockcroft, and A. Mitcheil, "Freckle formation and freckle criterion in superalloy castings", Metallurgical and Materials Transactions B, 31 (4) pp. 801 811, 2000.

[3]   D. Ma. Q. Wu, and A. B. Polaczek, "The Influence of Surface Roughness on Freckle Formation in Directionally Solidified Superalloy Samples", Metallurgical and Materials Transactions B, 43 (2) pp. 344 353, 2012.

[4]   J. Valdés, P. King, and X. B. Liu, "On the Formulation of a Freckling Criterion for Ni-Based Superalloy Vacuum Arc Remelting Ingots", Metallurgical and Materials Transactions A, 41 (9) pp. 2408 2416, 2010.

[5]   M. C. Flemings, et al, "MACROSEGREGATION. PT. 1", AIME Met Soc Trans, 239 (9) pp. 1449-1461, 1967.

[6]   M. C. Flemings, et al, "MACROSEGREGATION. PT. 2", AIME Met Soc Trans, 242 (1) pp. 41-49, 1968

[7]   R. Mehrabian, M. Keane, and M. C. Flemings, "Interdendritic Fluid Flow and Macrosegregation; Influence of Gravity", Materials Transactions, 1 (5) pp. 1209 1220, 1970.

[8]   R. Mehrabian, M. Keane, and M. C. Flemings, "Experiments on Macrosegregation and Freckle Formation", Materials Transactions, 1 (11) pp. 3238-3241, 1970.

[9]   W. H. Yang, W. chen, K. M. Chang, "FRECKLES IN REMELTED NIOBIUM CONTAINING SUPERALLOYS", Superalloys 718, 625, 706 and various derivatives, ed. E.A. Loria, TMS, pp. 113-122, 2001.

[10] W. H. Yang, W. Chen, K. M. Chang, S. Mannan, and J. deBarbadillo, "Freckle criteria for the upward directional solidification of alloys", Metallurgical and Materials Transactions A, 32 (2) pp. 397-406, 2001.

[11] W. H. Yang, John J. deBarbadillo, K. Morita, T. Suzuki, W. Chen, K. M. Chang, "A freckle criterion for the solidification of superalloys with a tilted solidification front", JOM, 56 (9) pp. 56 61, 2004.

[12] X. H. Wang, R. M. Ward, M. H. Jacobs, and M. D. Barratt, "Effect of Variation in Process Parameters om the Formation of Freckle in INCONEL 718 by Vacuum Arc Remelting", Metallurgical and Materials Transactions A, 39 (12) pp. 2981-2989, 2008.

[13] Y. Amouyal, D. N. Seidman, "An atom-probe tomographic study of freckle formation in a nickel-based superalloy", Acta Materialia, 59 (17) pp. 6729-6742, 2011.

[14] N. Shevchenko, S. Boden, G. Gerbeth, S. Eckert, "Chimney Formation in Solidifying Ga-25wt pct In

Alloys Under the Influence of Thermosolutal Melt Convection", Metallurgical and Materials Transactions A, 44 (8) pp. 3797-3808, 2013.

[15] R. J. Siddall, "Comparison of the Attributes of VIM+ESR and VIM+ESR Alloy 718", Superalloys 1991, Ed, E. A. Loria, TMS, pp. 29-41, 1991.

[16] K. O. Yu and J. A. Domingue, "CONTROL OF SOLIDIFICATION STRUCTURE IN VAR AND ESR PROCESSED ALLOY 718 INGOTS", Superalloys 1989, Ed, E. A. Loria, TMS, pp. 33-48, 1989.

[17] A. D. Helms, C. B. Adasczik, and L. A. Jackman, "EXTENDING THE SIZE LIMITS OF CAST/WROUGHT SUPERALLOY INGOTS", Superalloys 1996, Ed, R. D. Kissinger, TMS, pp. 427-433, 1996

[18] K.O. Yu, J.A Domingue, G.E. Maurer, and H.D. Flanders, "Macrosegregation in ESR and VAR processes", JOM, 38 (1) pp. 46-50, 1986

[19] Z. D. Long, X. B Liu, W. H. Yang, K. M. Chang, E. Barbero, "Thermodynamic assessment of liquid composition change during solidification and its effect on freckle formation in superalloys", Materials Science and Engineering: A, 386 (1) pp. 254-261, 2004.

[20] J. A, V. D. Avyle, J. A. Brooks, and A. C. Powell, "Reducing Defects in Remelting processes for High-performance alloys", JOM, 50 (3) pp. 22-25, 1998.

[21] P. D. Jablonski, C. J. Cowen, "Homogenizing a nickel-based superalloy: thermodynamic and kinetic simulation and experimental results", Metallurgical and Materials Transactions B, 40 (2) pp. 182-186, 2009.

[22] Q. Chen and B. Sundman, "Computation of partial equilibrium solidification with complete interstitial and negligible substitutional solute back diffusion", Materials Transactions, 43 (3) pp. 551 559, 2002.

[23] Z. Guo, N. Saunders, A.P. Miodownik, J. P. Schillé, "Modelling of materials properties and behaviour critical to casting simulation", Materials Science and Engineering: A, 413 pp. 465-469, 2005.

[24] Z. Guo, N. Saunders, A. P. Miodownik, J. P. Schillé, "Modeling material properties of lead-free solder alloys", Journal of Electronic Materials, 37 (1) pp. 23-31, 2008.

[25] D. R. Poirier, "Permeability for flow of interdendritic liquid in columnar-dendritic alloys", Metallurgical and Materials Transactions B, 18 (1) pp. 245-256, 1987.

[26] Y. NATSUME, M. D. TAKAHASHI, K. KAWASHIMA, E. TANIGAWA and K. OHSASA, "Evaluation of Permeability for Columnar Dendritic Structures by Three-dimensional numerical Flow Analysis" ISIJ International, 54 (2) pp. 3238-3241, 2014.

[27] M. E. Bealy and B.G. Thomas, "Prediction of dendrite arm spacing for low alloy steel casting processes", Metallurgical and Materials Transactions B, 27 (4) pp. 1209-1220, 1996.

[28] Z. Guo, N. Saunders, A. P. Miodownik, J. P. Schillé, "Introduction of Materials Modelling into Processing simulation-Towards True Virtual Design and simulation", International Journal of Metallurgical Engineering, 2 (2) pp. 198-202, 2013.

[29] S. Karagadde, L. Yuan, N. Shevchenko, S. Eckert, P. D. Lee. "3-D microstructural model of freckle formation validated using in situ experiments", Acta Materialia, 79 pp. 168-180, 2014.